

- the aperture, so IUE always observes maximum event emission around CMLs of  $\sim 150^\circ$  to  $270^\circ$  (2, 19, 21).
25. With observations 1 month after Jupiter opposition, the solar wind conditions could be ballistically extrapolated from Earth to Jupiter (19) with IMP-8 and GEOTAIL satellite data. The solar wind measured at Earth on 19 and 20 May should have reached Jupiter on 31 May. Over 17 to 21 May, the velocity decreased from  $\sim 600$  to  $\sim 400$  km s $^{-1}$ , the ram pressure was about average, and there were no significant magnetic field perturbations. The ballistic projection was confirmed (within  $\sim 1$  day) with magne-

- tometer data from the Galileo Orbiter. On May 1994, Galileo was  $\sim 1.7$  AU from Jupiter at a  $\sim 17^\circ$  Jupiter-sun-Galileo angle, and did not detect any magnetic field perturbations that could have reached Jupiter on  $\sim 28$  to 31 May 1994 [K. Khurana, private communication (1996)].
26. We are grateful to A. Storrs at the Space Telescope Science Institute (STScI) for his efforts in scheduling these WFPC2 GTO observations and to B. McCollum and the IUE staff at Goddard Space Flight Center for scheduling and execution of the IUE observations on short notice. G.E.B. is also grateful to I. Engle, F. Bagenal, L. Ben Jaffel, R. Thorne, D.

Rego, R. Clauer, and A. Ridley for helpful conversations; K. Khurana for providing the Galileo data, and the referees for helpful suggestions. This research was supported by the Jet Propulsion Laboratory 959122 and NASA ADP NAG5-3044 grants to the University of Michigan. This work was based on observations with the NASA-European Space Agency HST, obtained at the STScI, which is operated by the Association of Universities for Research in Astronomy for NASA under contract NAS5-26555.

12 July 1996; accepted 26 September 1996

## Direct Imaging of the Atomic Configuration of Ultradispersed Catalysts

P. D. Nellist and S. J. Pennycook\*

Direct imaging of individual catalyst metal atoms on the insulating surface of an industrial support is demonstrated. Individual platinum and rhodium atoms ultradispersed on  $\gamma$ -Al $_2$ O $_3$  supports were imaged by high-resolution Z-contrast (atomic number Z) microscopy in a 300-kilovolt scanning transmission electron microscope. Within small clusters, the configuration of the metal atoms was seen to be constrained to match the surface structure of the  $\gamma$ -Al $_2$ O $_3$ , from which likely surface adsorption sites were deduced. A thin, extended raft of rhodium atoms was observed, mostly corresponding to one monolayer. Occasional two-atom features suggested partial dissolution into the top layers of the  $\gamma$ -Al $_2$ O $_3$  support.

Direct observation of the atomic dispersion of a catalytic metal on its support material is essential for the understanding of catalytic activity and degradation mechanisms. The two systems presented here, platinum and rhodium supported on  $\gamma$ -Al $_2$ O $_3$ , have been extensively studied. Measurements of chemical activity (1) and x-ray absorption experiments (2) have demonstrated atomic dispersions approaching the limit of isolated metal atoms. However, to date no experimental investigations have provided definitive evidence of the metal atom configurations or their interactions with the support material (3). We used Z-contrast atomic-resolution imaging to directly observe the positions of the individual metal atoms on an industrial catalyst support material. Their configuration and orientation with respect to the support material can be determined, and information on their three-dimensional configuration can be extracted.

A Z-contrast image is formed in a scanning transmission electron microscope (STEM) by focusing an electron probe on the specimen and detecting electrons that scatter out to an annular dark-field detector. It is an incoherent mode that leads to a direct map of atomic locations with intensities that are strongly dependent on the

atomic number Z of the observed atom (4). Thus, it is an excellent method for observing supported metal atoms; indeed, in a biological context, this was one of the earliest applications of STEM (5). Later work has shown how atoms of different atomic number can be distinguished (6) and how the number of atoms in a column can be determined from the quantization of image intensities (7). Although the contrast of single atoms in Z-contrast images is much stronger than that in conventional TEM images, which can only image particles smaller than about 1 nm in diameter under special conditions (8), these previous Z-contrast results were only possible through the use of very thin, low-Z supports such as amorphous carbon films. With industrially relevant supports such as SiO $_2$  or  $\gamma$ -Al $_2$ O $_3$ , single atom detection has not been possible

until now because of the larger background scattering from these heavier supports. Nevertheless, the enhanced ability of Z-contrast imaging to distinguish between metal atoms and a support has made it a popular choice in the study of industrial catalysts. Hitherto, clusters as small as three atoms have been detectable (9), although the individual atoms could not be resolved.

The recently developed, high-resolution VG Microscopes HB603U 300-kV STEM (coefficient of spherical aberration of 1 mm) allows the formation of an electron probe only 0.126 nm in diameter. The resulting improved signal-to-background ratio from single atoms allows the resolution of individual metal atoms in tiny clusters on industrial catalyst supports. It is also possible in a STEM to form a bright-field (BF) image simultaneously with the Z-contrast image by detecting electrons collected by a small detector on the optical axis. By the principle of reciprocity (10), the BF image is identical to that which would be formed in a conventional TEM with the usual axial illumination. This image, being dominated by the support, is useful for determining the orientation of the support.

The ability of the microscope to resolve single atoms is illustrated in Fig. 1 for a sample of ultradispersed 3 weight % Pt on  $\gamma$ -Al $_2$ O $_3$ . The bright features (Fig. 1A) are clusters of Pt atoms. In many areas, the individual Pt atoms are resolved, showing that some clusters actually contain as few as two Pt atoms. The larger bright features are three-dimensional structures that are unresolved because they are not aligned accu-

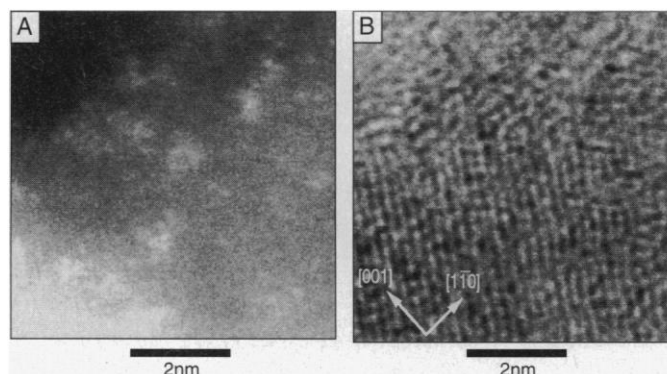


**Fig. 1.** Simultaneously collected (A) Z-contrast and (B) BF images of a sample of Pt on  $\gamma$ -Al $_2$ O $_3$ . Some of the clusters in (A) can be seen to be resolved into single atoms. In (B), strong {222}  $\gamma$ -Al $_2$ O $_3$  fringes can be seen with a spacing of 0.23 nm.

Solid State Division, Oak Ridge National Laboratory, Oak Ridge, TN 37831-6031, USA.

\*To whom correspondence should be addressed.

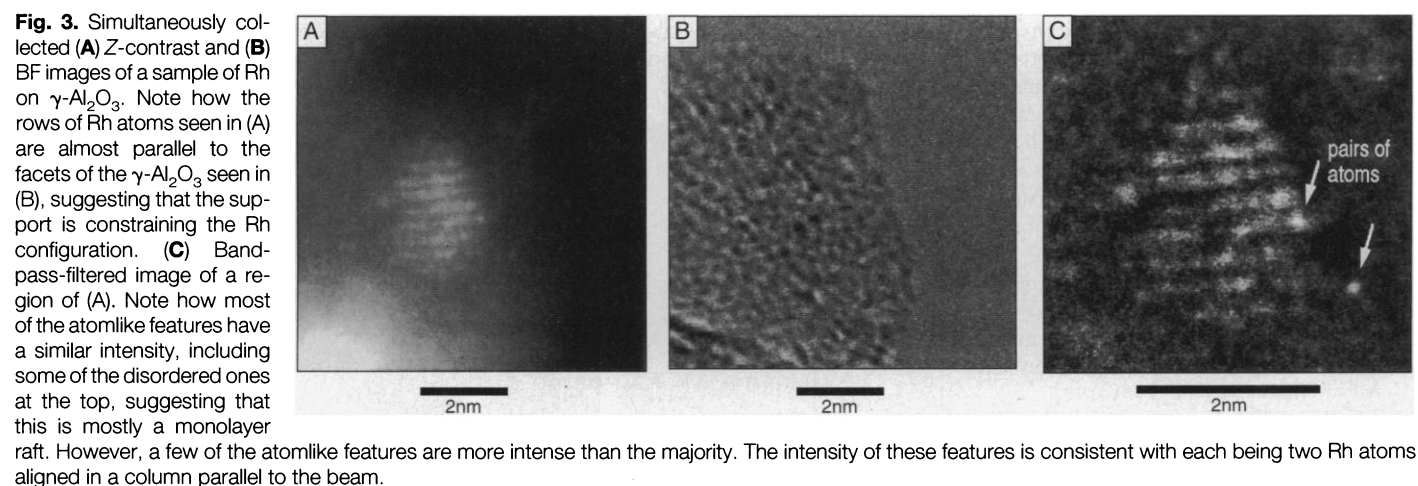
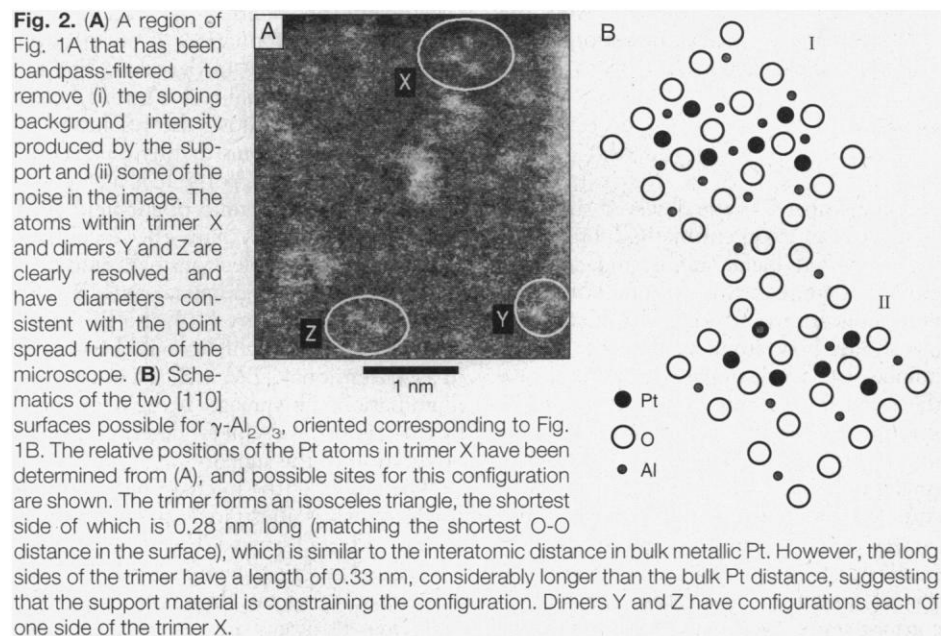
rately in the beam direction. Because the density of the Pt clusters is independent of the thickness of the support material, they must be associated with its surface. In contrast, the BF image (Fig. 1B) does not show any evidence of the Pt clusters, as expected considering the ultradispersed nature of this specimen. A Fourier transform of the BF image showed four peaks in intensity, indexed as the {222} reflections, from which the beam direction was determined to be near [110]. Indeed, the fringes resulting from some of these reflections can be seen in Fig. 1B, and from these the orientation of the alumina could be determined and the magnification of both images could be refined.

A common feature in dark-field images of this sample is the formation of triangular trimers of Pt atoms (labeled X in Fig. 2A). This trimer appears to form an isosceles triangle, rather than the close-packed equi-

lateral triangle that might be expected. Image distortions and drift, which are easily estimated from Fig. 1B, cannot account for this shape. Thus, we infer that the Pt configuration is somewhat constrained by the support surface. The relative coordinates of the Pt atoms in this trimer were determined by a maximum entropy analysis (11), and the relative coordinates of atoms in the two different types of [110] surface of the  $\gamma$ -Al<sub>2</sub>O<sub>3</sub> were determined from the orientation and magnification information contained in the BF image. Although the image data do not reveal the exact position of the trimer relative to the surface, Fig. 2B suggests possible configurations with the Pt atoms in sites doubly coordinated by the oxygen ions of the alumina and with Pt-O distances consistent with the 0.268-nm distances determined by x-ray absorption measurements (12). Analysis of other similar trimers and dimers gave relative Pt coordi-

nates within  $\pm 0.02$  nm of those for the trimer X; for example, the dimers labeled Y and Z in Fig. 2A each have the same spacing and orientation as the two atoms forming the corresponding side of trimer X. It is important to note that we can assume these structures exist on flat [110] terraces. If atoms in the trimers and dimers were located on different terraces, the atoms would be too far apart to be bonded, and trimers would form only through chance positional correlations. Because the trimers and dimers analyzed have such similar relative Pt coordinates and because isolated atoms are rarely observed, placement on different terraces is unlikely to be the case. It is interesting to note that the isosceles triangle displayed by the Pt atoms can also be seen in the Al lattice of the surface labeled I in Fig. 2B. As an alternative to the removal of incorporated H, substitution of Pt for Al in the surface could possibly explain the short 0.228-nm Pt-O distances observed in the x-ray measurements (12).

A more extensive arrangement of metal atoms is shown in Fig. 3A, a specimen of 1.2 weight % Rh on  $\gamma$ -Al<sub>2</sub>O<sub>3</sub>. Again, the arrangement of atoms visible in the Z-contrast image (Fig. 3A) is not visible in the BF image (Fig. 3B), suggesting that, although the feature is about 2 nm in diameter, it is an extremely thin raft-like structure. The Rh atoms are arranged in rows approximately parallel to the facets of the support (Fig. 3B), showing again an interaction with the support. Although the support was not oriented correctly to allow the imaging of BF lattice fringes to determine its orientation, the approximately 0.3-nm spacing and square arrangement of the Rh atoms are similar to those of the O sublattice in a [100] surface of  $\gamma$ -Al<sub>2</sub>O<sub>3</sub>. The ability to image the Rh atomic arrangement, even though the support is not crystallographically aligned with the beam, also indicates its two-dimensionality. Figure 3C has been



bandpass-filtered to remove the slowly varying background intensity produced by the support and shows how some of the atom features are distinctly more intense than the majority. The column intensity distribution is predominantly bimodal, with the more intense features having a mean intensity 2.5 times that of the majority. The intensity of the disordered single atoms visible at the top of the raft in Fig. 3C calibrates the intensity distribution. The more intense features are then consistent with two atoms arranged vertically in a column, because the resultant partially coherent scattering raises the intensity ratio above 2.

It is at first sight surprising that the isolated feature in the lower right of Fig. 3C and some of the atom sites at the edge of the raft should contain two atoms in a column. The absence of neighboring single-height columns raises the question of how these features are supported on the surface. A possible explanation is that some Rh atoms have been absorbed into the first layer of the alumina lattice, which would then allow the possibility of isolated pairs of Rh atoms arranged in a single column. Indeed, Yao *et al.* (13) have suggested disso-

lution of Rh into  $\gamma$ -Al<sub>2</sub>O<sub>3</sub> as a degradation mechanism, a view that is supported by these observations.

Recently, first-principle calculations have been successfully applied to catalytic systems (14). It should now be possible, using the information from high-resolution Z-contrast microscopy, to calculate the electronic structure of the observed metal cluster configurations and relate it to the catalytic activity experimentally observed. Researchers could also study directly the mechanisms of catalyst degradation by imaging a series of specimens. We believe that the information about the metal support configuration now available in the microscope will facilitate a more detailed understanding of catalyst activity and degradation mechanisms.

#### REFERENCES AND NOTES

1. For example, L. Spenadel and M. Boudart, *J. Phys. Chem.* **64**, 204 (1960); S. F. Adler and J. J. Keavney, *ibid.*, p. 208.
2. Reviewed by D. C. Koningsberger and B. C. Gates [*Catal. Lett.* **14**, 271 (1992)].
3. For example, A. S. Fung, P. A. Tooley, M. J. Kelley, D. C. Koningsberger, B. C. Gates, *J. Phys. Chem.* **95**, 225 (1991).

4. D. E. Jesson and S. J. Pennycook, *Proc. R. Soc. London Ser. A* **449**, 273 (1995).
5. A. V. Crewe, J. Wall, J. Langmore, *Science* **168**, 1338 (1970).
6. M. S. Isaacson, D. Kopf, M. Ohtsuki, M. Utlaut, *Ultramicroscopy* **4**, 101 (1979).
7. M. S. Isaacson, M. Ohtsuki, M. Utlaut, in *Introduction to Analytical Electron Microscopy*, J. J. Hren, J. Goldstein, D. C. Joy, Eds. (Plenum, New York, 1979), pp. 343-368.
8. S. Iijima, *Optik* **48**, 193 (1977); A. K. Datye and D. J. Smith, *Catal. Rev. Sci. Eng.* **34**, 129 (1992).
9. M. M. J. Treacy and S. B. Rice, *J. Microsc.* **156**, 211 (1989).
10. J. M. Cowley, *Appl. Phys. Lett.* **15**, 58 (1969); E. Zeitler and M. G. R. Thomson, *Optik* **31**, 258 (1970).
11. A. J. McGibbon, S. J. Pennycook, D. E. Jesson, *J. Microsc.*, in press.
12. D. C. Koningsberger and M. Vaarkamp, *Physica B* **208-209**, 633 (1995).
13. H. C. Yao, S. Japar, M. Shelef, *J. Catal.* **50**, 407 (1977).
14. R. Shah, M. C. Payne, M.-H. Lee, J. D. Gale, *Science* **271**, 1395 (1996).
15. We thank D. R. Liu and E. Lowenthal for the provision of the catalyst samples. This work was performed at Oak Ridge National Laboratory, which is managed by Lockheed Martin Energy Research for the U.S. Department of Energy under contract DE-AC05-96OR22464, through an appointment to the Oak Ridge National Laboratory Postdoctoral Program administered by the Oak Ridge Institute for Science and Education.

28 May 1996; accepted 13 August 1996

## Crystal Structure of DNA Recombination Protein RuvA and a Model for Its Binding to the Holliday Junction

John B. Rafferty, Svetlana E. Sedelnikova, David Hargreaves, Peter J. Artymiuk, Patrick J. Baker, Gary J. Sharples, Akeel A. Mahdi, Robert G. Lloyd, David W. Rice\*

The *Escherichia coli* DNA binding protein RuvA acts in concert with the helicase RuvB to drive branch migration of Holliday intermediates during recombination and DNA repair. The atomic structure of RuvA was determined at a resolution of 1.9 angstroms. Four monomers of RuvA are related by fourfold symmetry in a manner reminiscent of a four-petaled flower. The four DNA duplex arms of a Holliday junction can be modeled in a square planar configuration and docked into grooves on the concave surface of the protein around a central pin that may facilitate strand separation during the migration reaction. The model presented reveals how a RuvAB-junction complex may also accommodate the resolvase RuvC.

Recombination is a potent evolutionary force that shapes and reshapes the genomes of all organisms. More than 30 years ago, Holliday (1) proposed a model of meiotic recombination in which homologous chro-

matids exchange single DNA strands to form a partially heteroduplex joint molecule with a four-way junction at the point of exchange (Fig. 1A). Resolution of the Holliday junction by symmetrical strand cleavage, coupled with repair of any DNA base pair mismatches in the heteroduplex regions, provided a plausible explanation for the formation of recombinants and for the patterns of marker segregation in genetic crosses. Although many features of the model have since been found wanting, the idea that recombinant chromosomes arise

through the formation and subsequent resolution of Holliday intermediates has withstood the test of time (2). The reaction pathway has been dissected in detail in *Escherichia coli* (3). Eukaryotic homologs and analogs of the *E. coli* proteins are emerging (4-6), which leads to the expectation that the key features of the reaction mechanism will be generally, if not universally, applicable.

In the *E. coli* pathway, RecA protein polymerizes on single-strand tails at DNA ends or at single-strand gaps to form a helical nucleoprotein filament that promotes pairing and strand exchange with a homologous duplex (7). Strand exchange into regions of duplex-duplex pairing creates a Holliday intermediate that is then processed into mature products by RuvA, RuvB, and RuvC (8). RuvA and RuvB act in concert to provide a junction-specific DNA helicase that catalyzes branch migration (9-12). RuvA binds to the junction point (9, 10) where it targets the assembly of RuvB, a hexameric ring helicase that provides the motor to drive the reaction (13). Electron micrographs of the tripartite complex reveal RuvA sandwiched between two diametrically opposed RuvB rings (14). Parsons *et al.* (14) suggested that the junction is held in a square-planar configuration with the two RuvB rings assembled around homologous arms and facing each other (Fig. 1B). Rotation of the duplex DNA by RuvB provides a simple model of how

J. B. Rafferty, S. E. Sedelnikova, D. Hargreaves, P. J. Artymiuk, P. J. Baker, D. W. Rice, Krebs Institute, Department of Molecular Biology and Biotechnology, University of Sheffield, Western Bank, Sheffield S10 2TN, UK. G. J. Sharples, A. A. Mahdi, R. G. Lloyd, Department of Genetics, University of Nottingham, Queen's Medical Centre, Nottingham, NG7 2UH, UK.

\*To whom correspondence should be addressed. E-mail: d.rice@sheffield.ac.uk